crystals

MDPI

*Article*

# Structural Characterization, Magnetic and Luminescent Properties of Praseodymium(III)-4,4,4-Trifluoro-1-(2-Naphthyl)Butane-1,3-Dionato(1-) Complexes

**Franz A. Mautner [1,*], Florian Bierbaumer [1], Roland C. Fischer [2], Ramon Vicente [3], Ànnia Tubau [3], Arnau Ferran [3] and Salah S. Massoud [4,5,*]**

1 Institut für Physikalische and Theoretische Chemie, Technische Universität Graz, Stremayrgasse 9/II, A-8010 Graz, Austria; bierbaumerflorian97@gmail.com
2 Institut für Anorganische Chemie, Technische Universität Graz, Stremayrgasse 9/V, A-8010 Graz, Austria; roland.fischer@tugraz.at
3 Departament de Química Inorgànica i Orgànica, Universitat de Barcelona, Martí i Franquès 1-11, E-31321 Barcelona, Spain; rvicente@ub.edu (R.V.); anniatubau@ub.edu (À.T.); arferrasa@gmail.com (A.F.)
4 Department of Chemistry, University of Louisiana at Lafayette, P.O. Box 43700, Lafayette, LA 70504, USA
5 Department of Chemistry, Faculty of Science, Alexandria University, Moharem Bey 21511, Egypt
* Correspondence: mautner@tugraz.at (F.A.M.); ssmassoud@louisiana.edu (S.S.M.)

**Abstract:** Four new Pr(III) mononuclear complexes of formula $[Pr(ntfa)_3(MeOH)_2]$ (**1**), $[Pr(ntfa)_3(bipy)_2]$ (**2**), $[Pr(ntfa)_3(4,4'\text{-}Mt_2bipy)]$ (**3**) and $[Pr(ntfa)_3(5,5'\text{-}Me_2bipy)]$ (**4**), where ntfa = 4,4,4-trifuoro-1-(naphthalen-2-yl)butane-1,3-dionato(1-), 5,5′-Me2bipy = 5,5′-dimethyl-2,2′-dipyridine, 4,4′-Mt2bipy = 4,4′-dimethoxy-2,2′-dipyridine, have been synthesized and structurally characterized. The complexes display the coordination numbers 8 for **1, 3** and **4**, and 10 for **2**. Magnetic measurements of complexes **1–4** were consistent with a magnetically uncoupled $Pr^{3+}$ ion in the $^3H_4$ ground state. The solid state luminescence studies showed that the ancillary chelating bipyridyl ligands in the **2–4** complexes greatly enhance the luminescence emission in the visible and NIR regions through efficient energy transfer from the ligands to the central $Pr^{3+}$ ion; behaving as "antenna" ligands.

**Keywords:** praseodymium(III); beta-diketonate anion; magnetic properties; luminescence; crystal structure; antenna effect



**Citation:** Mautner, F.A.; Bierbaumer, F.; Fischer, R.C.; Vicente, R.; Tubau, À.; Ferran, A.; Massoud, S.S. Structural Characterization, Magnetic and Luminescent Properties of Praseodymium(III)-4,4,4-Trifluoro-1-(2-Naphthyl)Butane-1,3-Dionato(1-) Complexes. *Crystals* **2021**, *11*, 179. https://doi.org/10.3390/cryst11020179

Academic Editors: Helmut Cölfen and Simona Binetti

Received: 6 January 2021
Accepted: 8 February 2021
Published: 11 February 2021



## 1. Introduction

The unique properties of lanthanide complexes to display characteristic narrow emission bands over a wide spectral range from ultraviolet (UV) to near infrared (NIR) regions and their long emission life times (microseconds to milliseconds timescale) [1–9] make them ideal candidates for many potential applications. The lanthanide complexes have been employed in light devices [10–17], solid state lasers [1,2,18], temperature probes [19–21] and in the construction of optical signal amplifiers in telecommunication networks [22,23] as well as in biomedical imaging (MRI) fields [24,25]. Moreover, complexes of Pr(III), Er(III) and Yb(III) containing the Schiff base $N^2$,$N^3$-bis(anthracen-9-ylmethylene)pyridine-2,3-diamine (SBL) showed in vitro cytotoxicity against some human cancer cell lines [26] and the role of Ln(III) complexes to bind, cleavage of DNA also in diagnosis, and monitoring the treatment of cancer disease was recently summarized [27]. In addition to these applications, the presence of large number of unpaired *f*-electrons and the large intrinsic magnetic anisotropy of the lanthanide compounds [3,28–32] utilized a useful way in the design of molecular magnetic materials (SMMs) [3,33–43].

The high surface positive charge density of $Ln^{3+}$ ions (charge/ionic radius) makes them behave as hard acids and consequently they prefer the coordination to hard Lewis bases. Although the intermolecular interaction forces of $Ln^{3+}$ with chelated ligand(s) are

electrostatic in nature, steric factors rather than electronic ones [44] dominate the geometry of the complexes and as a result, the $Ln^{3+}$ complexes containing the same ligand are usually all isostructural. The interactions of β-diketonato ligands with $Ln^{3+}$ produces thermodynamically stable complexes [9,17,40,41,43,45–48], where the coordinated β-diketonates act as efficient antenna ligands for lanthanides emitting in the visible and NIR region [1–4,6,17,36]. The resulting Ln(III)-β-diketonates complexes may display coordination numbers (C.N.) up to 12, but 8 and 9 are the most frequently observed C.N. with the $Ln^{3+}$ ions. In most of these complexes, the central $Ln^{3+}$ ion is coordinated to 3 bidentate-β-diketonate anions, resulting in the presence of several vacant coordination positions, which may be available for the interaction with various solvent molecules and/or ancillary ligands [36,48–51].

Since the early lanthanide elements (Ce-Pm) were not thoroughly investigated compared to the heavier series (Sm-Yb), the following study was undertaken to focus on one of these elements. Therefore, herein, we report the synthesis, structural characterization and magnetic behavior as well as the luminescence properties of the four praseodymium(III) complexes derived from 4,4,4-trifluoro-1-(2-naphthyl)butane-1,3-dionato(1-) (ntfa) and the ancillary ligands: 2,2′-bipyridine (bipy), 5,5′-dimethyl-2,2′-bipyridine (5,5′-$Me_2$bipy) and 4,4'-dimethoxy-2,2′-bipyridine (4,4′-$Mt_2$bipy) as well as MeOH.

## 2. Materials and Methods

### *2.1. Materials and Physical Measurements*

4,4,4-Trifluoro-1-(2-naphthyl)butane-1,3-dione, 2,2′-bipyridine (bipy), 5,5′-dimethyl-2,2′-bipyridine (5,5′-$Me_2$bipy) and 4,4′-dimethoxy-2,2′-bipyridine (4,4′-$Mt_2$bipy) were purchased from TCI. Praseodymium(III) nitrate hexahydrate was obtained from Strem Chemicals and the other chemicals were of analytical grade quality. Infrared spectra of solid complexes were recorded on a Bruker Alpha P (platinum-ATR-cap) spectrometer. Elemental microanalyses for complex **1** were performed at Atlantic Microlaboratory, Atlanta, Georgia and the rest of complexes were carried out with an Elementar Vario EN3 analyser.

### *2.2. Synthesis of the Complexes*

*[Pr(ntfa)$_3$(MeOH)$_2$]* **(1)**. A methanolic solution (10 mL) of $Pr(NO_3)_3 \cdot 6H_2O$ (435 mg, 1 mmol) was added to another methanolic solution (15 mL) containing 4,4,4-trifluoro-1-(2-naphthyl)-1,3-butanedione (Hntfa) (799 mg, 3 mmol) and sodium hydroxide (120 mg, 3 mmol). The mixture was stirred for 2 h at room temperature, filtered through celite and then allowed to crystalize at ambient temperature. The shiny crystals of [Pr(ntfa)$_3$(MeOH)$_2$] (**1**), which was separated after two days, were collected by filtration, and dried in air (yield: 760 mg, 75%). Anal. Calcd. for $C_{44}H_{32}F_9O_8Pr$ (1000.61 g/mol): C, 52.8; H, 3.2; N, 0.0. Found: C, 52.8; H, 3.3; N, 0.0%. Selected IR bands (ATR-IR, $cm^{-1}$): 3450 (w,br), 1601 (s), 1590 (s), 1568 (m), 1531 (m), 1516 (m), 1457 (m), 1354 (w), 1286 (s), 1251 (m), 1183 (s), 1125 (vs), 1075 (m), 1016 (m), 958 (w), 864 (m), 796 (vs), 763 (m), 683 (s).

*[Pr(ntfa)$_3$(bipy)$_2$]* **(2)**. [Pr(ntfa)$_3$(MeOH)$_2$] (103 mg, 0.103 mmol) was dissolved in 15 mL ethanol/acetone (4:1) and 2,2′-bipyridine (34 mg, 0.22 mmol) was dissolved in 15 mL ethanol/acetone (4:1). The two solutions were combined and stirred for approximately 2 h. The mixture was then filtered and allowed to crystallize at room temperature. After three days, white crystals of [Pr(ntfa)$_3$(MeOH)$_2$] were collected by filtration and dried in air (yield: 71 mg, 52%). Anal. Calcd. for $C_{62}H_{40}F_9N_4O_6Pr$ (1248.89 g/mol): C, 59.6; H, 3.2; N, 4.5. Found: C, 59.8; H, 3.3; N, 4.4%. Selected IR bands (ATR-IR, $cm^{-1}$): 1632 (m), 1612 (s), 1591 (m), 1567 (m), 1505 (m), 1460 (m), 1432 (w), 1384 (w), 1352 (w), 1284 (s), 1167 (m), 1067 (m), 1004 (m), 957 (m), 923 (w), 862 (w), 816 (w), 785 (s), 750 (s), 680 (s), 636 (w), 564 (m), 506 (w), 470 (m), 449 (w), 416 (m).

*[Pr(ntfa)$_3$(4,4′-Mt$_2$Bipy)]* **(3)**. [Pr(ntfa)$_3$(MeOH)$_2$] (150 mg, 0.15 mmol) and 4,4′-dimethoxy-2,2′-dipyridine (36 mg, 0.16 mmol) were dissolved in 30 mL ethanol/acetone mixture (4:1) and the solution was stirred for approximately to 2 h. The mixture was then filtered and allowed

to crystallize at room temperature. After five days, the resulting small green crystals, which were separated, were collected by filtration and dried in air (yield: 109 mg, 63%). Anal. Calcd. for $C_{54}H_{36}F_9N_2O_8Pr$ (1152.76 g/mol): C, 56.3; H, 3.1; N, 2.4. Found: C, 56.5; H, 3.0; N, 2.4%. Selected IR bands (ATR-IR, $cm^{-1}$): 1606 (s), 1591 (m), 1563 (m), 1526 (m), 1507 (m), 1461 (m), 1387 (w), 1354 (w), 1286 (s), 1266 (m), 1218 (w), 1122 (s), 1073 (w), 1024 (s), 956 (m), 935 (w), 858 (w), 790 (s), 748 (m), 682 (s), 566 (s), 519 (m), 461 (m), 433 (w).

*[Pr(ntfa)$_3$(5,5′-Me$_2$Bipy)]* **(4)**. [Pr(ntfa)$_3$(MeOH)$_2$] (160 mg, 0.16 mmol) and 5,5′-dimethyl-2,2′-dipyridine (32 mg, 0.17 mmol) were dissolved in 20 mL ethanol/acetone mixture (3:1) and the solution was stirred for about 2 h at room temperature. The mixture was then filtered and allowed to crystallize at room temperature. After ten days, the green crystals, which were separated, were collected by filtration and dried in air (yield: 90 mg, 50%). Anal. Calcd. for $C_{54}H_{36}F_9N_2O_6Pr$ (1120.76 g/mol): C, 57.9; H, 3.2; N, 2.5. Found: C, 57.7; H, 3.3; N, 2.6%. Selected IR bands (ATR-IR, $cm^{-1}$): 1606 (s), 1588(m), 1567 (m), 1528 (m), 1506 (m), 1458 (m), 1384 (w), 1354 (w), 1289 (s), 1249 (m), 1219(w), 1181 (m), 1131 (s), 1072 (w), 956 (m), 935 (w), 865 (w), 793 (s), 751 (m), 680 (m), 563 (m), 518 (w), 471 (m), 392 (w).

### *2.3. Single Crystal X-ray Diffraction Analysis*

Single-crystal data of **1–4** were measured on an APEX II CCD diffractometer (Bruker-AXS). Table 1 summarizes crystallographic data, intensity data collection, and structure refinement specifications. Data collections were performed at 100(2) K with Mo–Kα radiation (λ = 0.71073 Å); computer programs APEX and SADABS [52,53] were used for data reduction, LP, and absorption corrections. The program library SHELX [54,55] was used for solution (direct methods) and refinement (full-matrix least-squares methods on $F^2$). Anisotropic displacement parameters were applied to all non-hydrogen atoms. H atoms (Uiso) were obtained from difference Fourier maps. HFIX geometrical constraints were applied only for C–H bonds. Additional software: Mercury [56]; PLATON [57]. CCDC deposition numbers: CCDC 2054083 for **1**, CCDC 2054084 for **2**, CCDC 2054085 for **3**, and CCDC 2054086 for **4**.

**Table 1.** Crystallographic data and processing parameters for **1–4**.

| **Compound** | **1** | **2** |
|---|---|---|
| Empirical formula | $C_{44}H_{32}F_9O_8Pr$ | $C_{62}H_{40}F_9N_4O_6Pr$ |
| Formula mass | 1000.61 | 1248.89 |
| System | Monoclinic | Triclinic |
| Space group | $P2_1/c$ | P-1 |
| a (Å) | 8.9307(4) | 11.9059(4) |
| b (Å) | 28.9448(12) | 15.3694(5) |
| c (Å) | 16.2421(7) | 16.5675(6) |
| α (°) | 90 | 79.097(2) |
| β (°) | 105.674(2) | 70.308(2) |
| γ (°) | 90 | 67.575(2) |
| V ($Å^3$) | 4042.4(3) | 2632.08(16) |
| Z | 4 | 2 |
| *T* (K) | 100(2) | 100(2) |
| μ ($mm^{-1}$) | 1.301 | 1.016 |
| Dcalc ($Mg/m^3$) | 1.644 | 1.576 |
| θ max (°) | 30.110 | 27.000 |
| Data collected | 185055 | 95375 |

**Table 1.** *Cont.*

| **Compound** | **1** | **2** |
|---|---|---|
| Unique refl./Rint | 11862/0.0797 | 11469/0.0642 |
| Parameters/Restraints | 567/0 | 767/66 |
| Goodness-of-Fit on $F^2$ | 1.234 | 0.991 |
| R1/wR2 (all data) | 0.0437/0.0853 | 0.0276/0.0728 |
| **Compound** | **3** | **4** |
| Empirical formula | $C_{54}H_{36}F_9N_2O_8Pr$ | $C_{54}H_{36}F_9N_2O_6Pr$ |
| Formula mass | 1152.76 | 1120.76 |
| System | Monoclinic | Orthorhombic |
| Space group | $P2_1/c$ | $Pca2_1$ |
| a (Å) | 13.2021(5) | 20.1848(6) |
| b (Å) | 14.6509(6) | 11.9034(3) |
| c (Å) | 24.8108(10) | 19.6102(6) |
| α (°) | 90 | 90 |
| β (°) | 98.938(2) | 90 |
| γ (°) | 90 | 90 |
| V ($Å^3$) | 4740.7(3) | 4711.7(2) |
| Z | 4 | 4 |
| *T* (K) | 100(2) | 100(2) |
| μ ($mm^{-1}$) | 1.123 | 1.124 |
| Dcalc ($Mg/m^3$) | 1.615 | 1.580 |
| θ max (°) | 30.641 | 29.995 |
| Data collected | 405492 | 163636 |
| Unique refl./Rint | 14586/0.0514 | 13727/0.0648 |
| Parameters/Restraints | 669/0 | 651/7 |
| Goodness-of-Fit on $F^2$ | 1.146 | 1.029 |
| R1/wR2 (all data) | 0.0260/0.0622 | 0.0266/0.0534 |

### *2.4. Powder X-ray Diffraction*

The purity of the compounds was checked by PXRD (See Supplement Materials Figures S1–S4). The powder patterns were measured on a Bruker D8 Advance diffractometer (Bruker AXS, Madison, WI, USA) with a LynxEye detector in Bragg–Brentano θ/θ geometry, with the sample dispersed thinly on a zero-background Si sample holder, λ(CuKα) = 1.54060 Å, scans from 5° to 50° 2θ, stepsize 0.02°.

### *2.5. Magnetic Measurements*

Magnetic measurements were performed on solid polycrystalline samples in a Quantum Design MPMS-XL SQUID magnetometer at the Magnetic Measurements Unit of the Universitat de Barcelona. Pascal's constants were used to estimate the diamagnetic corrections, which were subtracted from the experimental susceptibilities to give the corrected molar magnetic susceptibilities.

### *2.6. Luminescence Measurements*

Solid state fluorescence spectra were recorded on a Horiva Jobin Yvon SPEX Nanolog fluorescence spectrophotometer equipped with a three slit double grating excitation and emission monochromator with dispersions of 2.1 nm/mm (1200 grooves/mm) at room

temperature. The steady-state luminescence was excited by unpolarized light from a 450 W xenon CW lamp and detected at an angle of 90° for solid state measurement by a red-sensitive Hamamatsu R928P photomultiplier tube. Spectra were reference corrected for both the excitation source light intensity variation (lamp and grating) and the emission spectral response (detector and grating). Near infra-red spectra were recorded at an angle of 90° using a liquid nitrogen cooled, solid indium/gallium/arsenic detector (850–1600 nm).

## 3. Results and Discussion

### *3.1. Synthesis and Spectra*

The reaction of a methanolic solution of $Pr(NO_3)_3{\cdot}6H_2O$ with 4,4,4-trifluoro-1-(2-naphthyl)-butane-1,3-dione (Hntfa) in the presence of NaOH in a 1:3:3 molar ratio yielded the complex $[Pr(ntfa)_3(MeOH)_2]$ (**1**). The interaction of $[Pr(ntfa)_3(MeOH)_2]$ with the polypyridyl compounds bipy, $Me_2$bipy and $Mt_2$bipy afforded the title crystalline complexes $[Pr(ntfa)_3(bipy)_2]$ (**2**), $[La(ntfa)_3(Mt_2bipy)]$ (**3**) and $[Pr(ntfa)_3(Me_2bipy)]$ (**4**), respectively in moderate yields (50–63%). The isolated complexes **1–4** were structurally characterized by single crystal X-ray crystallography as well as by elemental microanalyses and by IR spectroscopy. Furthermore, their purity was checked by Powder X-ray diffraction (PXRD).

As expected, the IR spectra of the complexes **1–4** display a general characteristic feature. The strong vibrational band observed over the frequency range 1605–1615 $cm^{-1}$ is typically assigned to the coordinated carbonyl stretching frequency, ν(C=O) and the weak broad band observed around 3450 $cm^{-1}$ in **1** reveals the ν(O-H) stretching frequency of MeOH.

### *3.2. Description of the Crystal Structures* **(1–4)**

Molecular plots and coordination figures of **1–4** are depicted in Figures 1–4, respectively together with selected some bond distances and angles in each compound. Each Pr(III) center of the neutral and monomeric complexes **1–4** are ligated by six oxygen donor atoms of three β-diketonato ligand anions (ntfa). Coordination numbers (C.N.) eight around Pr1 in **1** is completed by oxygen atoms of two terminal methanol molecules, in **3** and **4** by two N-donor atoms of the chelating 4,4′-dimethoxy-dipyridine and 5,5′-dimethyl-2,2′-dipyridine, respectively. The Pr-O/N bond distances in **1**, **3** and **4** vary from 2.382(2) to 2.6455(13) Å. (C.N.) ten around Pr1 in **2** is completed by four nitrogen donor atoms of the two bipy chelating ligands. The Pr-N/O bond distances in **2** are in the range from 2.4527(15) to 2.8378(18) Å. The O-Pr1-O bite angles of the β-diketone groups fall in the range from 67.63(5) to 70.62(7)° in **1–4**, and the N-Pr1-N bite angles of the chelating bipy, Mtbipy and $Me_2$bipy molecules in **2–4** vary from 56.80(5) to 61.81(9)°.

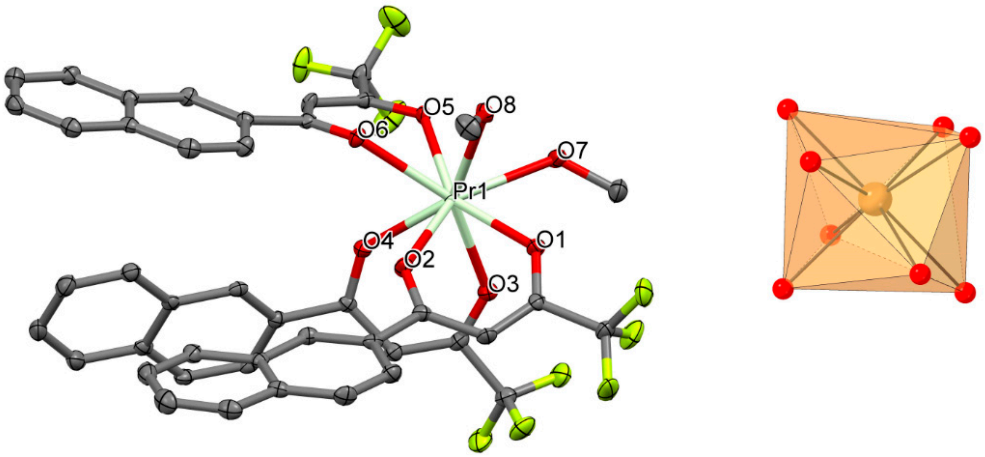


**Figure 1.** Perspective view (**left**) and coordination figure (**right**) of **1**. Selected bond distances (Å) and bond angles (°): Pr1-O1 2.395(2), Pr1-O2 2.416(2), Pr1-O3 2.408(2), Pr1-O4 2.382(2), Pr1-O5 2.462(2), Pr1-O6 2.453(2), Pr1-O7 2.498(2), Pr1-O8 2.586(2); O1-Pr1-O2 70.62(7), O3-Pr1-O4 69.72(7), O5-Pr1-O6 68.79(7).

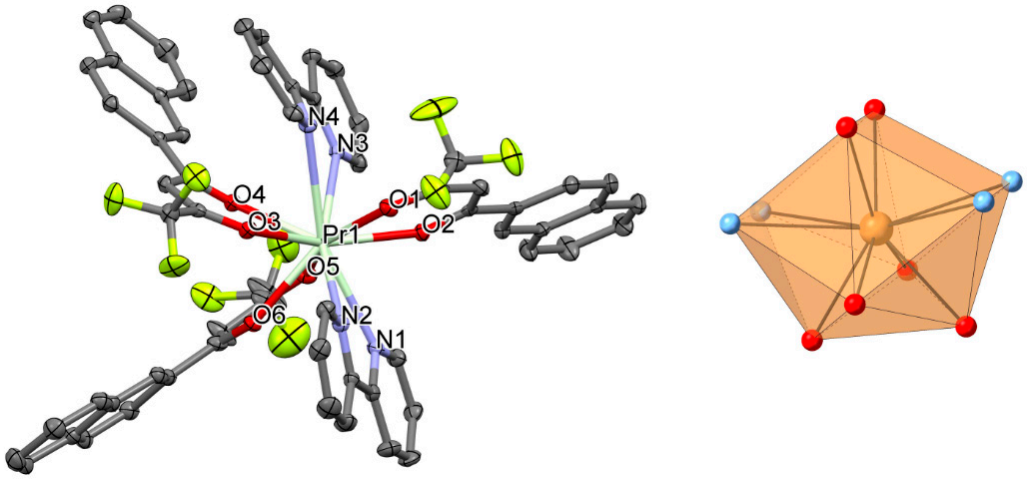


**Figure 2.** Perspective view (**left**) and coordination figure (**right**) of **2**. Selected bond distances (Å) and bond angles (°): Pr1-O1 2.5131(15), Pr1-O2 2.4614(14), Pr1-O3 2.4770(14), Pr1-O4 2.4531(14), Pr1-O5 2.4527(15), Pr1-O6 2.4651(14), Pr1-N1 2.7792(18), Pr1-N2 2.7434(17), Pr1-N3 2.8045(17), Pr1-N4 2.8378(18); O1-Pr1-O2 67.63(5), O4-Pr1-O3 68.65(5), O6-Pr1-O5 69.09(5), N1-Pr1-N2 58.10(5), N3-Pr1-N4 56.80(5).

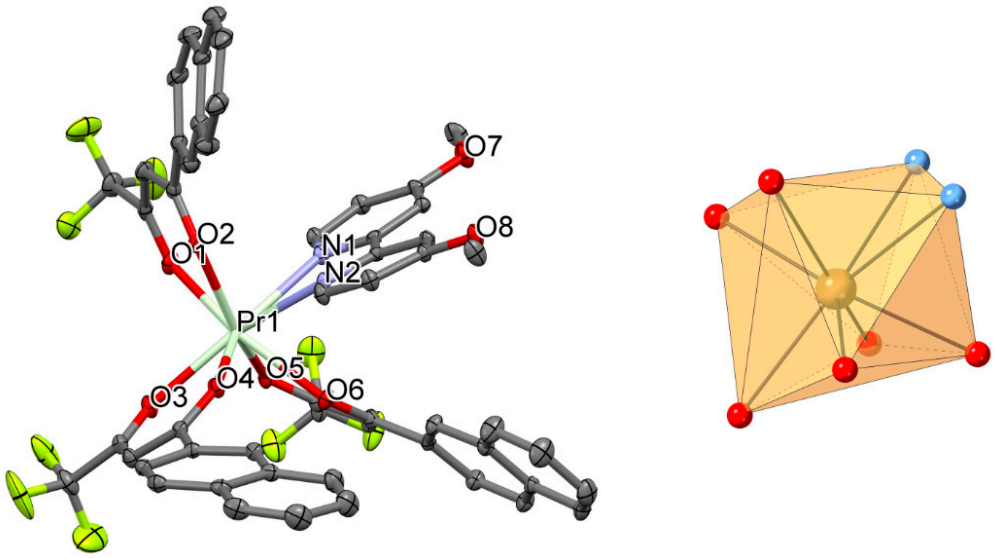


**Figure 3.** Perspective view (**left**) and coordination figure (**right**) of **3**. Selected bond distances (Å) and bond angles (°): Pr1-O1 2.4035(12), Pr1-O2 2.4610(12), Pr1-O3 2.4499(12), Pr1-O4 2.4036(11), Pr1-O5 2.4300(12), Pr1-O6 2.4045(11), Pr1-N1 2.6284(13), Pr1-N2 2.6455(13); O1-Pr1-O2 69.80(4), O3-Pr1-O4 69.50(4), O5-Pr1-O6 69.59(4), N1-Pr1-N2 60.34(4).

The calculation of the degree of distortion of the $PrO_8$ coordination polyhedron for **1** with respect to ideal eight-vertex polyhedra, using the continuous shape measure theory and SHAPE software [58,59], shows intermediate distortion between various coordination polyhedra. The lowest continuous shape measures (CShM's) values for compound **1** correspond to triangular dodecahedron (TDD-8), biaugmented trigonal prism (BTPR-8) and square antiprism (SAPR-8), with values of 0.379, 1.714 and 2.491, respectively. The corresponding values for the $PrO_6N_2$ coordination polyhedra for **3** are 0.877, 2.737 and 3.401; and for **4** are 0.933, 2.005 and 2.348, respectively. The calculation of the degree of distortion of the $PrO_6N_4$ coordination polyhedron for **2** with respect to ideal ten-vertex polyhedra shows intermediate distortion between various coordination polyhedra. The lowest continuous shape measures (CShM's) values for compound **2** correspond to Sphe-

nocorona J87 (JSPC-10) with a value of 0.427. The next lowest continuous shape measures correspond to Bicapped square antiprism J17 (JBCSAPR-10) with a value of 4.041.

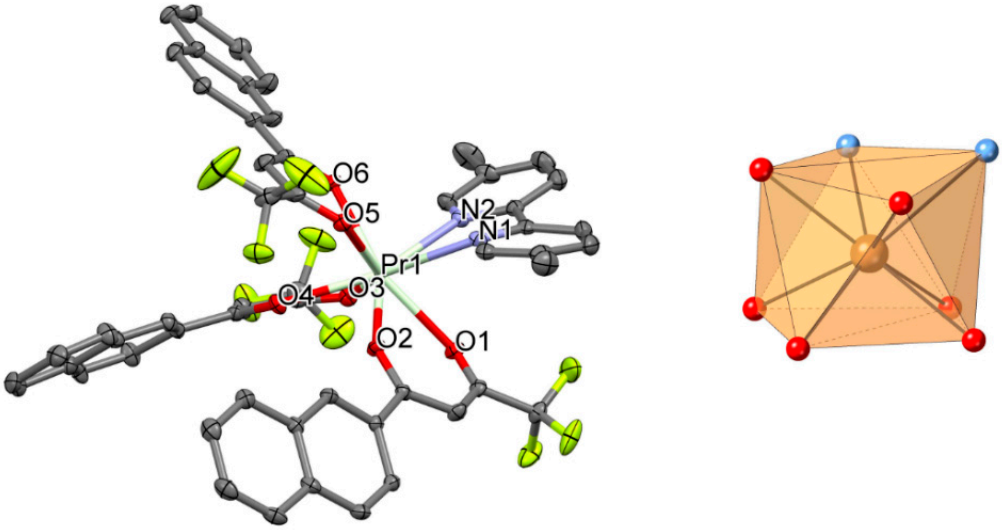


**Figure 4.** Perspective view (**left**) and coordination figure (**right**) of **4**. Selected bond distances (Å) and bond angles (°): Pr1-O1 2.436(2), Pr1-O2 2.392(2), Pr1-O3 2.425(2), Pr1-O4 2.416(2), Pr1-O5 2.426(2), Pr1-O6 2.410(2), Pr1-N1 2.630(3), Pr1-N2 2.632(3); O1-Pr1-O2 68.88(7), O3-Pr1-O4 70.00(7), O5-Pr1-O6 69.60(8), N1-Pr1-N2 61.81(9).

Packing plots of **1–4** compounds are presented in Figures S5–S8 in the supplementary section. The O-H groups of the MeOH molecules in **1** form hydrogen bonds of type O-H···O to generate centrosymmetric dimeric units. The aromatic naphthyl- (in **1–4**) and pyridyl- (in **2–4**) moieties are involved in numerous π···π ring···ring and C-H/F···ring interactions which further stabilize the packing of the mononuclear complexes (Tables S1–S4). Interestingly in the packing of **3** a stacking sequence of four naphthyl moieties is observed where the π···π ring···ring interactions connect the 4 mononuclear complexes within the unit cell to a secondary building unit (SBU) (Figure S7).

There exist two types of conformers with respect to the relative orientations of the three ntfa ligands. In complexes **1** and **3** with conformer A the three ntfa ligands are oriented in the same direction, whereas in **2** and **4** one ntfa ligand has opposite orientation compared to the other two ones (conformer B).

The Pr-O/N bond distances in structure of [Pr(ntfa)3(phen)] (phen = 1,10-phenanthroline) [60] vary from 2.388(2) to 2.694(3) Å, average 2.487 Å. Eight-coordinated Pr(III) in title compounds **1**,**3** and **4** have mean Pr-O/N bond distances of 2.450, 2.478 and 2.471 Å, respectively, whereas a mean Pr-O/N bond length of 2.599 Å is found in the complex **2** with C.N. ten. Title compounds **2** and **4** are isomorphic to their corresponding La(III) complexes [49] with mean La-O/N bond distances of 2.634 and 2.581 Å, respectively. In contrast to title complex **1**, as a consequence of larger ionic size, three MeOH molecules are ligated to La(III) to form $[La(ntfa)_3(MeOH)_3]$ with a mean La-O bond length of 2.539 Å for C.N. 9.

### *3.3. Magnetic Properties*

Powder samples of complexes **1–4** were measured under applied magnetic fields of 0.3 T over the temperature rang 300–2 K. The data are plotted as $\chi_M T$ products versus $T$ in Figure 5. The Magnetization dependence of the applied field at 2 K were also recorded and shown in Figure 6. The magnetic measurements on the **1–4** complexes reveal that the $\chi_M T$ values at 300 K are 1.47, 1.76, 1.66 and 1.38 $cm^3 \cdot mol^{-1} \cdot K$, respectively, which are in the range of the theoretical value for a magnetically uncoupled Pr(III) compound (1.60 $cm^3 \cdot mol^{-1} \cdot K$) in the $^3H_4$ ground state (g = 4/5). Upon cooling the **1–4** compounds, the $\chi_M T$ values decrease gradually reaching the same value of 0.05 $cm^3 \cdot mol^{-1} \cdot K$ at 2 K.

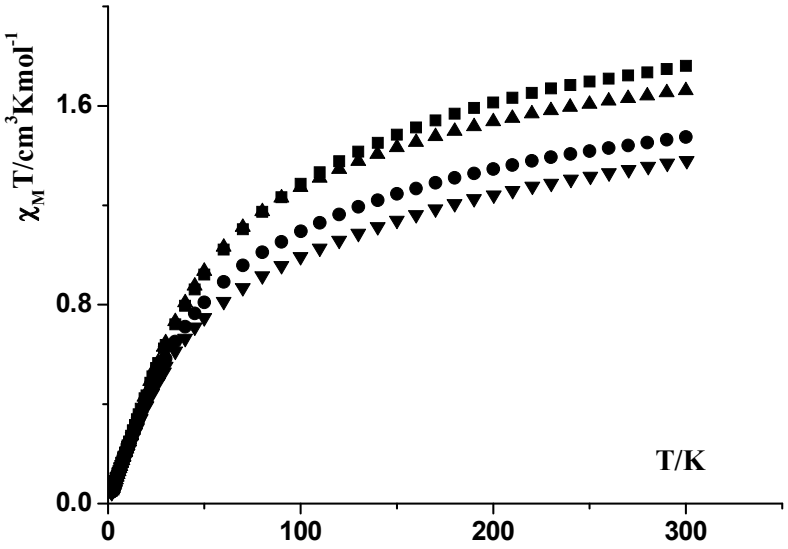


**Figure 5.** $\chi_M T$ vs. $T$ plots for compounds **1** (●), **2** (■), **3** (▲) and **4** (▼).

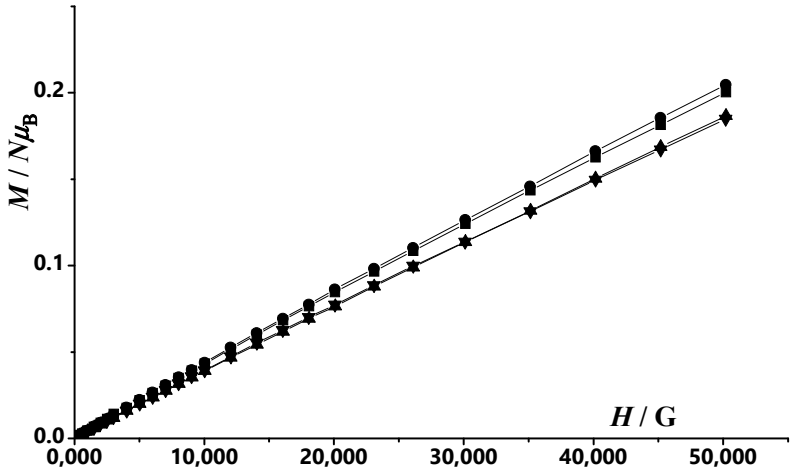


**Figure 6.** Field dependence of the magnetization plots at $T$ = 2 K for compounds: **1** (●), **2** (■), **3** (▲) and **4** (▼). The solid ines are a guide fot the eye.

Magnetization dependence on magnetic static applied field at $T$ = 2 K for complexes **1–4** (Figure 6) reveals no saturation at high fields with similar values of 0.20, 0.20, 0.19 add 0.18 $N\mu_B$ at 5T for **1–4** complexes, respectively.

The $1/\chi_M$ values were plotted against T for the **1–4** compounds and plots are shown in Figure 7. Between 45 and 300 K, the $1/\chi_M$ versus $T$ plots are linear for the four compounds and well described by the Curie–Weiss law $1/\chi_M = (T - \theta)/C$, where C = 1.76 $cm^3 \cdot mol^{-1} \cdot K$ and $\theta = -60.4$ K for **1**, C = 2.6 $cm^3 \cdot mol^{-1} \cdot K$ and $\theta = -104$ K for **2**, C = 1.96 $cm^3 \cdot mol^{-1} \cdot K$ and $\theta = -54.6$ K for **3** and C = 1.7 $cm^3 \cdot mol^{-1} \cdot K$ and $\theta = -66$ K for **4**. Comparable results were obtained for the previously published [$(\eta_2$(N,N)-3,5-*t*$Bu_2$dp$)_3$Pr(THF)$_2$] compound (C = 1.527 $cm^3 \cdot mol^{-1} \cdot K$ and $\theta = -70.24$ K), where [K(3,5-*t*$Bu_2$dp)] = potassium 3,5-di-*tert*-butyl-1,2,4-diazaphospholide [61].

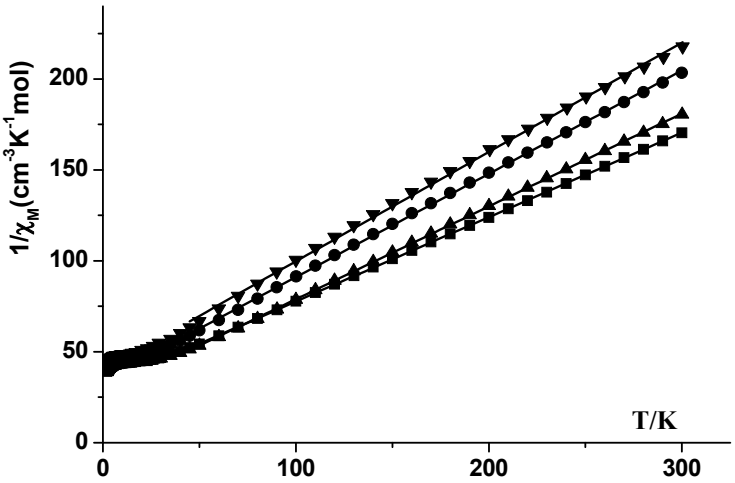


**Figure 7.** $1/\chi_M$ vs. $T$ plots for compounds **1** (●), **2** (■), **3** (▲) and **4** (▼).

### *3.4. Luminescence Properties*

The luminescence properties of the compounds under investigation were studied in the solid state at room temperature. In all compounds, the excitation spectra reveal the presence of an intense band around 350 nm, which corresponds to the $\pi \rightarrow \pi^*$ transition from the ligands. The emission spectra were recorded at the excitation wavelengths ($\lambda_{ex}$) of 350 nm for **1** and **4**, 330 nm for **2** and 340 nm for **3**. The excitation emission spectra of all compounds are illustrated in Figure 8.

For $[Pr(ntfa)_3(MeOH)_2]$ (**1**), very weak emission bands were observed around 596 and 606 nm, which are attributed to the *f-f* transitions in the $Pr^{3+}$ ion and a broad intense band at 454 nm corresponding to the ligand emission showing a non-effective antenna effect. The presence of two coordinated methanol molecules bonded to the central $Pr^{3+}$ ion in the coordination sphere of **1** and their involvement in H-bonding in the vicinity of the metal center are strongly quench the luminescence through non-radiative relaxation processes, especially through the vibrational quenching caused by O–H vibrations [62].

The luminescence emission spectra of the complexes **2**–**4** display general characteristic features, where four emission bands were observed around 596, 610, 618 nm and a fourth one was located at 635, 632 and 625 nm for complexes **2**, **3** and **4**, respectively (Figure 8). These emission bands result from the *f-f* transitions of the $Pr^{3+}$ ion in these compounds. The two intense bands centered at 610 and 618 nm were assigned to the $^1D_2 \rightarrow {}^3H_4$ and $^3P_0 \rightarrow {}^3H_6$, respectively in the three complexes **2**–**4**, whereas the medium intense band located around 630 ± 5 nm was most likely assigned to the $^3P_0 \rightarrow {}^3F_2$ transition. In addition, each complex displays a pair of emission bands in the near Infrared (NIR) region at 1025, 1061 nm for complex **2**, 1010, 1061 nm for **3** and 615, 1061 nm for **4**. These bands arise from the $^1D_2$ level and can be assigned to the $^1D_2 \rightarrow {}^3F_4$ transition for the lower energy band and tentatively to $^1D_2 \rightarrow {}^3F_2$ transition for the former band in each complex [63]. Probably, it should be noted that luminescence band located at 1061 nm was previously assigned to $^1G_4 \rightarrow {}^3H_4$ transition but due to the absence of conclusive information, it was assigned to $^1D_2 \rightarrow {}^3F_4$ transition [64]. Similar NIR emission bands with very weak intensities were also detected in **1**. As expected, displacement of the coordinated MeOH in **1** by the ancillary strong chelating ligands bipy, 4,4′-$Mt_2$bipy or 5,5′-$Me_2$bipy in complexes **2, 3** or **4**, respectively, led to significant enhancement of the luminescent intensities. Each complex of the series **2**–**4** displayed three strong emission bands of about close intensity at 610, 618 and 1061 nm. The positions and almost all of the intensities of the observed bands are independent of the nature of the ancillary ligands.

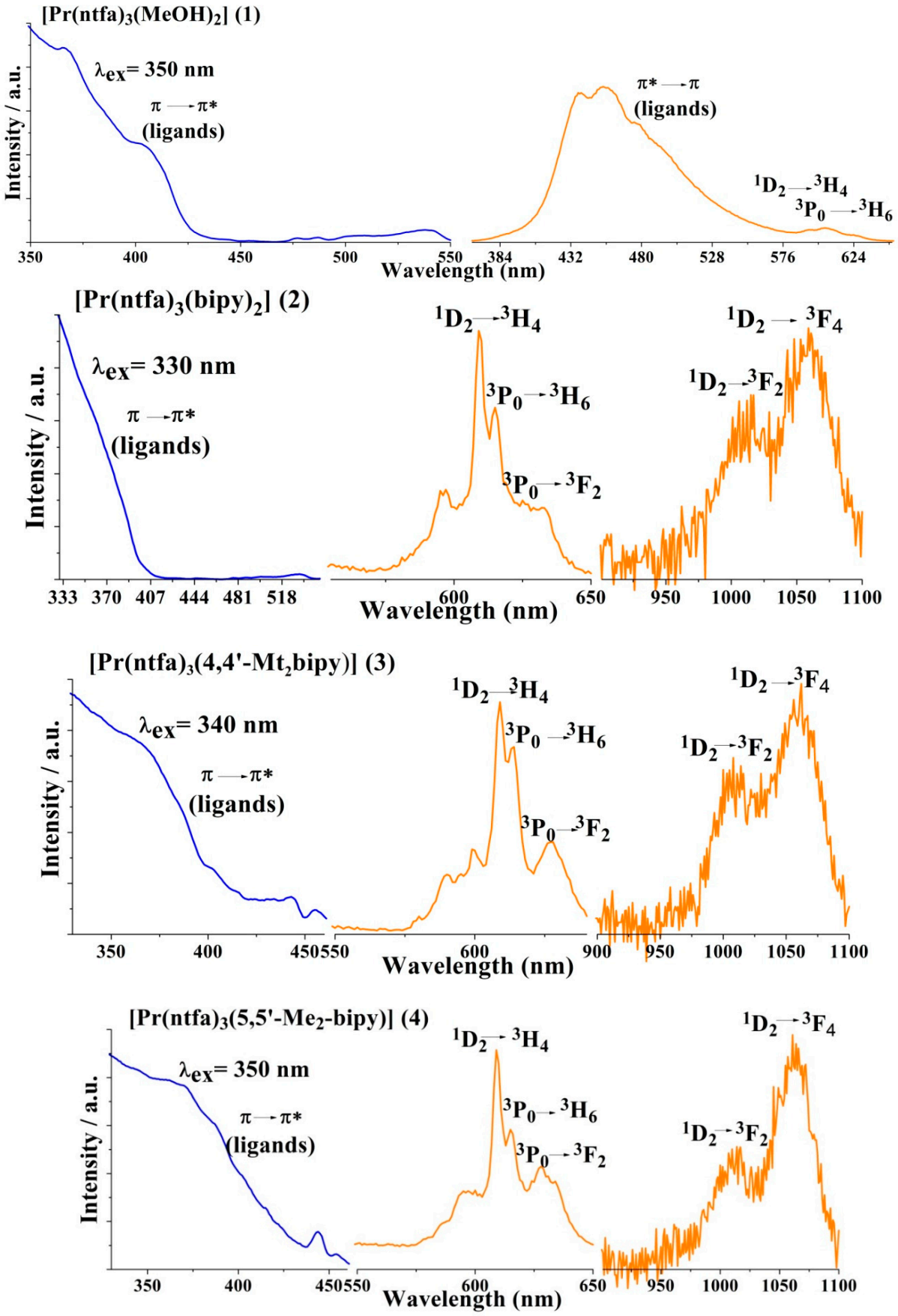


**Figure 8.** Excitation (blue line) and emission (orange line) of compounds **1–4** recorded in the solid state at room temperature.

The assignments of the emission bands in the four complexes were based on comparison of the *f-f* transitions of the $Pr^{3+}$ ion in compounds **2–4** with some similar chelated Pr($\beta$-diketonato)$_3$ systems [65,66] and their corresponding *f-f* energy levels scheme [67]. Moreover, it has been reported that the excited $Pr^{3+}$ may lose energy in the cross-relaxation process $Pr^{3+}$ ($_1D^2$) + $Pr^{3+}$ ($_3H^4$) → $Pr^{3+}$($_1G^4$) + $Pr^{3+}$($_3F^4$) [68,69], in addition the luminescence is generated by two different excited states, $^3P_0$ and $^1D_2$. This is common for $Pr^{3+}$ ions when the ligand triplet state is considerably higher than the $^3P_0$ and $^1D_2$ energy levels. Thus, in the compounds **2–4**, there is an efficient intramolecular energy transfer from the ligand's triplet state to the excited states of $Pr^{3+}$ ion. The results obtained here are similar to those reported in related $Pr^{3+}$ compounds and $Pr^{3+}$-$\beta$-diketonates systems [60,63,70,71].

## 4. Conclusions

Three mononuclear Pr(III) complexes of C.N 8 in [Pr(ntfa)$_3$(MeOH)$_2$] (**1**), [Pr(ntfa)$_3$(4,4′-Mt$_2$bipy)] (**3**) and [Pr(ntfa)$_3$(5,5′-Me$_2$bipy)] (**4**) as well as C.N. 10 in [Pr(ntfa)$_3$(bipy)$_2$] (**2**) have been synthesized and structurally characterized. Interestingly, steric demand encountered in substituted 2,2′-bipyrdine derivatives led to the formation of mono-adducts as this was demonstrated in compounds **3** and **4** as well as [Pr(ntfa)$_3$(phen)] [60], whereas as un-substituted bipy forms a bis(bipy) adduct as occurred in the case in [Pr(ntfa)$_3$(bipy)$_2$] (**2**). Probably the O-H···O hydrogen bonding in **1** and the generated dimeric units supressed the possibility of formation of a compound with C.N. > 8. However, it has been reported that the ability of the lanthanide (III) ions to form C.N. 8–10 with the same ligand set decreases across the series and the ability to isolate complexes with C.N. > 8 is not very common in the late lanthanide series but it can be targeted through stoichiometry and under solvent-free syntheses and this approach was demonstrated in the syntheses of [Ln(hfac)$_3$(bipy)$_2$] and [Ln(hfac)$_3$(bipy)] complexes from the [Ln(hfac)$_3$($H_2O$)$_3$], where Ln = La-Sm and hfac = 1,1,1,5,5,5-hexafluoro-acetylacetonate anion [72]. In addition, Pr(III) complexes with C.N. 10 were isolated and characterized in a series of heterodimetallic Pr(III) complexes of acetylacetonate derivatives containing small anions such as $NO_3^-$ [73–75].

The magnetic measurements of the four complexes **1–4** revealed that the $\chi_M T$ values at 300 K are within the range of 1.60 $cm^3 \cdot mol^{-1} \cdot K$, which is predicted for magnetically uncoupled Pr(III) compounds ($4f^2$) in the $^3H_4$ ground state. Similar magnetic behavior was observed in [Pr(hfac)3(NITFumbis)] {NITFumbis = (2,5-bis-(1-oxido-4,4′,5′,5′-tetramethyl-4,5-hydro-1H-imidazol-2-yl)furan} molecules, where the C.N. = 8 [41]. The luminescence studies of the complexes showed that binding the "antenna" ligands to the $Pr^{3+}$ ion resulted in a strong absorption of the ligand in the UV region and efficient energy transfer from the ligands to the central Pr(III) ion. Replacement of the coordinated MeOH in **1** by strong chelating bipyridyl ligands (bipy, 4,4′-Mt$_2$bipy or 5,5′-Me$_2$bipy), significantly enhances the luminescent intensities in the visible and NIR regions, where the complexes **2–4** revealed strong emission bands at 610, 618 and 1061 nm, which are almost independent of the nature of the ancillary bipyridyl ligands. The luminescence emission and magnetic results reported here indicate that these properties are not significantly affected by either the C.N. of the Pr(III) complexes nor their local symmetry, however, this is not the case in the late lanthanide series [41].

**Supplementary Materials:** The following are available online at https://www.mdpi.com/2073-4352/11/2/179/s1, Figures S1–S4: PXRD data of compounds **1–4**, Figures S5–S8: packing plots of compounds **1–4**, Tables S1–S4: Non-covalent intractions of **1–4.**

**Author Contributions:** Investigation, F.B. (synthesis and IR spectra)., R.C.F. (single crystal structures), À.T., A.F. (luminescence), F.A.M. (powder diffraction) and R.C.F. (magnetism); validation, F.A.M., R.V., R.C.F. and S.S.M.; writing—original draft preparation, F.A.M., F.B., R.C.F., R.V., À.T., A.F. and S.S.M.; writing—review and editing, F.A.M., À.T., R.V. and S.S.M.; project administration, F.A.M., R.V. and S.S.M.; funding acquisition, R.V. All authors have read and agreed to the published version of the manuscript.

**Funding:** This work was supported by Ministerio de Ciencia, Innovación y Universidades (Spain), Project PGC2018-094031-B-100. The APC was funded by Technische Universität Graz.

**Acknowledgments:** A.T., A.F. and R.V. acknowledge the financial support: "Open Access Funding by the Graz University of Technology".

**Conflicts of Interest:** The authors declare no conflict of interest.

## References

1. Bünzli, J.-C.G. On the design of highly luminescent lanthanide complexes. *Coord. Chem. Rev.* **2015**, *293–294*, 19–47.
2. Bünzli, J.-C.G.; Piguet, C. Taking advantage of luminescent lanthanide ions. *Chem. Soc. Rev.* **2005**, *34*, 1048–1077. [CrossRef]
3. Jia, J.-H.; Li, Q.-W.; Chen, Y.-C.; Liu, J.-L.; Tong, M.-L. Luminescent single-molecule magnets based on lanthanides: Design strategies, recent advances and magneto-luminescent studies. *Coord. Chem. Rev.* **2019**, *378*, 365–381. [CrossRef]
4. Armelao, L.; Quici, S.; Barigelletti, F.; Accorsi, G.; Bottaro, G.; Cavazzini, M.; Tondello, E. Design of luminescent lanthanide complexes: From molecules to highly efficient photo-emitting materials. *Coord. Chem. Rev.* **2010**, *254*, 487–505. [CrossRef]
5. Moore, E.G.; Xu, J.; Jocher, C.J.; Werner, E.J.; Raymond, K.N. Cymothoe sangaris: An extremely stable and highly luminescent 1,2-hydroxy-pyridinonate chelate of Eu(III). *J. Am. Chem. Soc.* **2006**, *128*, 10648–10649. [CrossRef]
6. Quici, S.; Cavazzini, M.; Marzanni, G.; Accorsi, G.; Armaroli, N.; Ventura, B.; Barigelletti, F. Visible and near-infrared intense luminescence from water-soluble lanthanide [Tb(III), Eu(III), Sm(III), Dy(III), Pr(III), Ho(III), Yb(III), Nd(III), Er(III)] complexes. *Inorg. Chem.* **2005**, *44*, 529–537. [CrossRef]
7. Petoud, S.; Cohen, S.M.; Bünzli, J.-C.G.; Raymond, K.N. Stable lanthanide luminescence agents highly emissive in aqueous solution: Multidentate 2-hydroxyisophthalamide complexes of $Sm^{3+}$, $Eu^{3+}$, $Tb^{3+}$, $Dy^{3+}$. *J. Am. Chem. Soc.* **2003**, *126*, 13324–13325. [CrossRef]
8. Bakker, B.H.; Goes, M.; Hoebe, N.; Van Ramesdonk, H.J.; Verhoeven, J.W.; Werts, M.H.V.; Hofstraat, J.W. Luminescent materials and devices: Lanthanide azatriphenylene complexes and electroluminescent charge transfer systems. *Coord. Chem. Rev.* **2000**, *208*, 3–16. [CrossRef]
9. Mara, D.; Artizzu, F.; Laforce, B.; Vincze, L.; Van Hecke, K.; Van Deun, R.; Kaczmarek, A.M. Novel tetrakis lanthanide β-diketonate complexes: Structural study, luminescence properties and temperature sensing. *J. Lumin.* **2019**, *213*, 343–355. [CrossRef]
10. Dai, P.-P.; Li, C.; Zhang, X.-T.; Xu, J.; Chen, X.; Wang, X.-L.; Jia, Y.; Wang, X.; Liu, Y.-C. A single Eu2+-activated high-color-rendering oxychloride white-light phosphor for white-light-emitting diodes. *Light Sci. Appl.* **2016**, *5*, e16024. [CrossRef]
11. Dai, P.; Lee, S.-P.; Chan, T.-S.; Huang, C.-H.; Chiang, Y.-W.; Chen, T.-M. $Sr_3Ce(PO_4)_3$: $Eu^{2+}$: A broadband yellow-emitting phosphor for near ultraviolet-pumped white light-emitting devices. *J. Mater. Chem.* **2016**, *C4*, 1170–1177. [CrossRef]
12. Zhong, J.; Chen, D.; Zhou, Y.; Wan, Z.; Ding, M.; Bai, W.; Ji, Z. New $Eu^{3+}$-activated perovskite $La_{0.5}Na_{0.5}TiO_3$ phosphors in glass for warm white light emitting diodes. *Dalton Trans.* **2016**, *45*, 4762–4770. [CrossRef] [PubMed]
13. Zhu, H.; Fang, M.; Huang, Z.; Liu, Y.G.; Chen, K.; Min, X.; Mao, Y.; Wang, M. Photoluminescence properties of $Li_2Mg_2$ $(WO_4)_3$: $Eu^{3+}$ red phosphor with high color purity for white LEDs applications. *J. Lumin.* **2016**, *172*, 180–184. [CrossRef]
14. Li, C.; Dai, J.; Huang, J.; Deng, D.; Yu, H.; Wang, L.; Ma, Y.; Hua, Y.; Xu, S. Crystal structure, luminescent properties and white light emitting diode application of $Ba_3GdNa(PO_4)_3F$: $Eu^{2+}$ single-phase white light-emitting phosphor. *Ceram. Int.* **2016**, *42*, 6891–6898. [CrossRef]
15. Pavitra, E.; Raju, G.S.R.; Ko, Y.H.; Yu, J.S. A novel strategy for controllable emissions from $Eu^{3+}$ or $Sm^{3+}$ ions co-doped $SrY_2O_4$: $Tb^{3+}$ phosphors. *Phys. Chem. Chem. Phys.* **2012**, *14*, 11296–11307. [CrossRef]
16. Lin, C.C.; Meijerink, A.; Liu, R.-S. Critical red components for next-generation white LEDs. *J. Phys. Chem. Lett.* **2016**, *7*, 495–503. [CrossRef]
17. Dar, W.A.; Ahmed, Z.; Iftikhar, K. Cool white light emission from the yellow and blue emission bands of the Dy(III) complex under UV excitation. *J. Photoch. Photobio. A* **2018**, *356*, 502–511. [CrossRef]
18. de Bettencourt-Dias, A. Lanthanide-based emitting materials in light emitting diodes. *Dalton Trans.* **2007**, *22*, 2229–2241. [CrossRef]
19. Brites, C.D.S.; Millan, A.; Carlos, L.D.; Bünzli, J.C.G.; Pecharsky, V.K. (Eds.) *Handbook of the Physics and Chemistry of Rare Earths, Lanthanides in Luminescent Thermometry*; Elsevier B.V.: Amsterdan, The Netherlands, 2016; Volume 49, Chapter 281, pp. 339–427.
20. An, R.; Zhao, H.; Hu, H.-M.; Wang, X.; Yang, M.-L.; Xue, G. Synthesis, structure, white light emission, and temperature recognition properties of Eu/Tb mixed coordination polymer. *Inorg. Chem.* **2016**, *55*, 871–876. [CrossRef]
21. Miyata, K.; Konno, Y.; Nakanishi, T.; Kobayashi, A.; Kato, M.; Fushimi, K.; Hasegawa, Y. Chameleon luminophore for sensing temperatures: Control of metal-to-metal and energy back transfer in lanthanide coordination polymers. *Angew. Chem. Int. Ed.* **2013**, *52*, 6413–6416. [CrossRef]
22. Oshishi, Y.; Kanamori, T.; Kitagawa, T.; Takashashi, S.; Snitzer, E.; Sigel, G.H. $Pr^{3+}$-doped fluoride fiber amplifier operating at 1.31 μm. *Opt. Lett.* **1991**, *16*, 1747–1749. [CrossRef] [PubMed]
23. Slooff, L.H.; Polman, A.; Wolbers, M.P.O.; van Veggel, F.; Reinhoudt, D.N.; Hofstraat, J.W. Optical properties of erbium-doped organic polydentate cage complexes. *J. Appl. Phys.* **1998**, *83*, 497–503. [CrossRef]
24. Surender, E.M.; Comby, S.; Martyn, S.; Cavanagh, B.; Lee, C.T.; Brougham, D.F.; Gunnlaugsson, T. Cyclen lanthanide-based micellar structures for application as luminescent [Eu(III)] and magnetic [Gd(III)] resonance imaging (MRI) contrast agents. *Chem. Commun.* **2016**, *52*, 1085–10861. [CrossRef]

25. Nchimi-Nono, K.; Wenger, K.D.; Linden, S.; Lecointre, A.; Ehret-Sabatier, L.; Shakir, S.; Hildebrandt, N.; Charbonniere, L.J. Activated phosphonated trifunctional chelates for highly sensitive lanthanide-based FRET immunoassays applied to total prostate specific antigen detection. *Org. Biomol. Chem.* **2013**, *11*, 6493–6501. [CrossRef]
26. Andiappan, K.; Sanmugam, A.; Deivanayagam, E.; Karuppasamy, K.; Kim, H.-S.; Vikraman, D. In vitro cytotoxicity activity of novel Schiff base ligand–lanthanide complexes. *Sci. Rep.* **2018**, *8*, 3054. [CrossRef] [PubMed]
27. Jastrza, R.; Nowak, M.; Skroban'ska, M.; Tolin'ska, A.; Zabiszak, M.; Gabryel, M.; Marciniak, Ł.; Kaczmarek, M.T. DNA as a target for lanthanide(III) complexes influence. *Coord. Chem. Rev.* **2019**, *382*, 145–159. [CrossRef]
28. Singh, S.K.; Gupta, T.; Rajaraman, G. Magnetic anisotropy and mechanism of magnetic relaxation in Er(III) single-ion magnets. *Inorg. Chem.* **2014**, *53*, 10835–10845. [CrossRef]
29. Takamatsu, S.; Ishikawa, T.; Koshihara, S.; Ishikawa, N. Significant increase of the barrier energy for magnetization reversal of a single-4f-ionic single-molecule magnet by a longitudinal contraction of the coordination space. *Inorg. Chem.* **2007**, *46*, 7250–7252. [CrossRef]
30. Ishikawa, N.; Sugita, M.; Wernsdorfer, W.G. Nuclear spin driven quantum tunneling of magnetization in a new lanthanide single-molecule magnet: Bis(phthalocyaninato)holmium anion. *J. Am. Chem. Soc.* **2005**, *127*, 3650–3651. [CrossRef]
31. Ishikawa, N.; Sugita, M.; Ishikawa, T.; Koshihara, S.Y.; Kaizu, Y. Lanthanide double-decker complexes functioning as magnets at the single-molecular level. *J. Am. Chem. Soc.* **2003**, *125*, 8694–8695. [CrossRef]
32. Benelli, C.; Caneschi, A.; Guillou, O.; Pardi, L. Synthesis, crystal structure, and magnetic properties of tetranuclear complexes containing exchange-coupled dilanthanide-dicopper (lanthanide = gadolinium, dysprosium) species. *Inorg. Chem.* **1990**, *29*, 1750–1755. [CrossRef]
33. Woodruff, D.N.; Winpenny, R.E.P.; Layfield, R.A. Lanthanide single-molecule magnets. *Chem. Rev.* **2013**, *113*, 5110–5148. [CrossRef] [PubMed]
34. Zhu, Z.; Li, X.-L.; Liuac, S.; Tang, J. External stimuli modulate the magnetic relaxation of lanthanide single-molecule magnets. *Inorg. Chem. Front.* **2020**, *7*, 3315–3326. [CrossRef]
35. Marin, R.; Brunet, G.; Murugesu, M. Shining new light on multifunctional lanthanide single-molecule magnets. *Angew. Chem.* **2019**, *60*, 1728–1746. [CrossRef] [PubMed]
36. Casanovas, B.; Speed, S.; Maury, O.; Font-Bardía, M.; Vicente, R. Homodinuclear lanthanide 9-anthracenecarboxylate complexes: Field induced SMM and NIR-luminescence. *Polyhedron* **2019**, *169*, 187–194. [CrossRef]
37. Dey, A.; Kalita, P.; Chandrasekhar, V. Lanthanide(III)-based single-ion magnets. *ACS Omega* **2018**, *3*, 9462–9475. [CrossRef] [PubMed]
38. Lu, J.; Guo, M.; Tang, J. Recent Developments in lanthanide single-molecule magnets. *Chem. Asian J.* **2017**, *12*, 2772–2779. [CrossRef]
39. Layfield, R.A.; Murugesu, M. (Eds.) *Lanthanides and Actinides in Molecular Magnetism*; Wiley-VCH Verlag GmbH & Co. KgaA: Weinheim, Germany, 2015.
40. Yao, X.; An, G.; Li, Y.; Yan, P.; Li, W.; Li, G. Effect of nuclearity and symmetry on the single-molecule magnets behavior of seven-coordinated β-diketonate Dy(III) complexes. *J. Solid State Chem.* **2019**, *274*, 295–302. [CrossRef]
41. Li, X.; Li, T.; Tian, L.; Liu, Z.Y.; Wang, X.G. Experimental and theoretical interpretation of the magnetic behavior of two Dy(III) single-ion magnets constructed through β-diketonate ligands with different substituent groups (–Cl/ $OCH_3$). *RSC Adv.* **2015**, *5*, 74864–74873. [CrossRef]
42. Zhang, P.; Zhang, L.; Wang, C.; Xue, S.; Lin, S.-Y.; Tang, J. Equatorially coordinated lanthanide single ion magnets. *J. Am. Chem. Soc.* **2014**, *136*, 4484–4487. [CrossRef] [PubMed]
43. Liu, C.-M.; Zhang, D.Q.; Zhu, D.-B. Field-induced single-ion magnets based on enantiopure chiral β-diketonate ligands. *Inorg. Chem.* **2013**, *52*, 8933–8940. [CrossRef]
44. Rizkalla, E.N. Systematics of lanthanide coordination. *Radiochim. Acta* **1993**, *61*, 181–188. [CrossRef]
45. Ansari, A.A.; Ganaie, A.B.; Iftikhar, K. Synthesis and 4f-4f absorption studies of tris(acetylacetonato) praseodymium(III) and holmium(III) complexes with imidazole and pyrazole in non-aqueous solvents. Structure elucidation by sparkle/PM7. *J. Mol. Struct.* **2019**, *1198*, 126826. [CrossRef]
46. Wang, W.-M.; Liu, S.-Y.; Xu, M.; Bai, L.; Wang, H.-Q.; Wen, X.; Zhao, X.-Y.; Qiao, H.; Wu, Z.-L. Structures and magnetic properties of phenoxo-O-bridged dinuclear lanthanide(III) compounds: Single-molecule magnet behaviour and magnetic refrigeration. *Polyhedron* **2018**, *145*, 114–119. [CrossRef]
47. Chen, G.-J.; Zhou, Y.; Jin, G.-X.; Dong, Y.-B. $[Dy(acac)_3(dppn)]\cdot C_2H_5OH$: Construction of a single-ion magnet based on the square-antiprism dysprosium(III) ion. *Dalton Trans.* **2014**, *43*, 16659–16665. [CrossRef] [PubMed]
48. Ansari, A.A.; Ilmi, R.; Iftikhar, K. Hypersensitivity in the 4f–4f absorption spectra of tris(acetylacetonato)neodymium(III) complexes with imidazole and pyrazole in non-aqueous solutions. Effect of environment on hypersensitive transitions. *J. Lumin.* **2012**, *132*, 51–60. [CrossRef]
49. Mautner, F.A.; Bierbaumer, F.; Gyurkac, M.; Fischer, R.C.; Torvisco, A.; Massoud, S.S.; Vicente, R. Synthesis and characterization of lanthanum(III) complexes containing 4,4,4-trifluoro-1-(2-naphthalen-yl)-butane-1,3-dionate. *Polyhedron* **2020**, *179*, 114384. [CrossRef]

50. Ansari, A.A.; Hussain, H.A.; Iftikhar, K. Optical absorption spectroscopic studies on holmium(III) complexes with β-diketone and heterocyclic amines. The environment effect on 4f–4f hypersensitive transitions. *Spectrochim. Acta Part A* **2007**, *68*, 1305–1312. [CrossRef] [PubMed]
51. Ansari, A.A.; Ahmed, Z.; Iftikhar, K. Nuclear magnetic resonance and optical absorption spectroscopic studies on paramagnetic praseodymium(III) complexes with β-diketone and heterocyclic amines. *Spectrochim. Acta Part A* **2007**, *68*, 176–183. [CrossRef] [PubMed]
52. *Bruker APEX, SAINT v. 8.37A*; Bruker AXS Inc.: Madison, WI, USA, 2015.
53. Sheldrick, G.M. *SADABS v. 2*; University of Goettingen: Goettingen, Germany, 2001.
54. Sheldrick, G.M. A Short history of SHELX. *Acta Crystallogr. A* **2008**, *64*, 112–122. [CrossRef] [PubMed]
55. Sheldrick, G.M. Crystal structure refinement with SHELXL. *Acta Crystallogr. C Struct. Chem.* **2015**, *71*, 3–8. [CrossRef] [PubMed]
56. Macrae, C.F.; Edington, P.R.; McCabe, P.; Pidcock, E.; Shields, G.P.; Taylor, R.; Towler, T.; van de Streek, J.J. Mercury: Visualization and analysis of crystal structures. *Appl. Cryst.* **2006**, *39*, 453–457. [CrossRef]
57. Spek, A.L. *PLATON, a Multipurpose Crystallographic Tool*; Utrecht University: Utrecht, The Netherlands, 1999.
58. Alvarez, S.; Alemany, P.; Casanova, D.; Cirera, J.; Llunell, M.; Avnir, D. Shape maps and polyhedral interconversion paths in transition metal chemistry. *Chem. Soc. Rev.* **2005**, *249*, 1693–1708. [CrossRef]
59. Cirera, J.; Alvarez, S. Stereospinomers of pentacoordinate iron porphyrin complexes: The case of the [Fe(porphyrinato)(CN)]$^{-}$ anions. *Dalton. Trans.* **2013**, *42*, 7002–7008. [CrossRef]
60. Yu, J.; Zhang, H.; Fu, L.; Deng, R.; Zhou, L.; Li, H.; Liu, F.; Fu, H. Synthesis, structure and luminescent properties of a new praseodymium(III) complex with β-diketone. *Inorg. Chem. Commun.* **2003**, *6*, 852–854. [CrossRef]
61. Zhao, M.; Wang, L.; Li, P.; Ma, J.; Zheng, W. 1,2,4-Diazaphospholide complexes of lanthanum(III), cerium(III), neodymium(III), praseodymium(III), and samarium(III): Synthesis, X-ray structural characterization, and magnetic susceptibility studies. *Dalton Trans.* **2016**, *45*, 11172–11181. [CrossRef]
62. Eliseeva, S.V.; Bünzli, J.C. Lanthanide luminescence for functional materials and bio-sciences. *Chem. Soc. Rev.* **2010**, *39*, 189–227. [CrossRef]
63. Voloshin, A.I.; Shavaleev, N.M.; Kazakov, V.P. Luminescence of praseodymium(III) chelates from two excited states ($^{3}P_0$ and $^{1}D_2$) and its dependence on ligand triplet state energy. *J. Lumin.* **2001**, *93*, 199–204. [CrossRef]
64. Sveshnikova, E.B.; Timofeev, N.T. Disruption of cascading of nonradiative transitions in the $Pr^{3+}$ ion. *Opt. Spektrosk.* **1980**, *48*, 503–509.
65. Kazakov, V.P.; Voloshin, A.I.; Shavaleev, N.M. Chemiluminescence in visible and infrared spectral regions and quantum chain reactions upon thermal and photochemical decomposition of adamantylideneadamantane-1,2-dioxetane in the presence of chelates $Pr(dpm)_3$ and $Pr(fod)_3$. *J. Photo Chem. Photobiol. A Chem.* **1998**, *119*, 177–186. [CrossRef]
66. Voloshin, A.I.; Shavaleev, N.M.; Kazakov, V.P. Chemiluminescence of praseodymium(III), neodymium (III) and ytterbium(III) β-diketonates in solution excited from 1,2-dioxetane decomposition and singlet–singlet energy transfer from ketone to rare-earth β-diketonates. *J. Lumin.* **2000**, *91*, 49–58. [CrossRef]
67. Carnall, W.T.; Fields, P.R.; Rajnak, K. Electronic energy levels of the trivalent Lanthanide aquo ions. III. $Tb^{3+}$. *J. Chem. Phys.* **1968**, *49*, 4424. [CrossRef]
68. Chrysochoos, J.; Qusti, A.H. Electronic relaxation of $^{3}P_0$ and $^{1}D_2$ states of Pr(3+) in $POCl_3$:$SnCl_4$. *J. Less Common Met.* **1986**, *126*, 169–174. [CrossRef]
69. Qusti, A.H.; Chrysochoos, J. Concentration and temperature dependence of the luminescence arising from $^{3}P_0$ and $^{1}D_2$-states of $Pr^{3+}$ in $POCl_3$:$SnCl_4$. *J. Less Common Met.* **1985**, *112*, 291–295. [CrossRef]
70. Davies, G.M.; Aarons, R.J.; Motson, G.R.; Jeffery, J.C.; Adams, H.; Faulkner, S.; Ward, M.D. Structural and near-IR photophysical studies on ternary lanthanide complexes containing poly(pyrazolyl)borate and 1,3-diketonate ligands. *Dalton Trans.* **2004**, *8*, 1136–1144. [CrossRef] [PubMed]
71. Pereira, V.M.; Costa, A.L.; Feldl, J.; Maria, T.M.R.; de Melo, J.S.; Martín-Ramos, P.; Martín-Gile, J.; Silva, R.M. Synthesis, structure and physical properties of luminescent Pr(III) β-diketonate complexes. *Spectrochim. Acta Part A Mol. Biomol. Spectrosc.* **2017**, *172*, 25–33. [CrossRef] [PubMed]
72. Fatila, E.M.; Maahs, A.C.; Hetherington, E.H.; Cooper, B.J.; Cooper, R.E.; Daanen, N.N.; Jennings, M.; Skrabalak, S.E.; Preuss, K.E. Stoichiometric control: 8- and 10-coordinate Ln(hfac)3(bpy) and Ln(hfac)3(bpy)2 complexes of the early lanthanides La–Sm†. *Dalton Trans.* **2018**, *47*, 16232–16241. [CrossRef] [PubMed]
73. Shiga, T.; Ohba, M.; Ōkawa, H. A Series of Trinuclear $Cu^{II}Ln^{III}Cu^{II}$ complexes derived from 2,6-di(acetoacetyl)pyridine: synthesis, structure, and magnetism. *Inorg. Chem.* **2004**, *43*, 4435–4446. [CrossRef]
74. Joan Gónzalez-Fabra, J.; Bandeira, N.A.G.; Velasco, V.; Barrios, L.A.; David Aguilà, D.; Teat, S.J.; Roubeau, O.R.; Bo, C.; Aromí, G. Thermodynamic stability of heterodimetallic [LnLn] complexes: Synthesis and DFT Studies. *Chem A Eur. J.* **2017**, *23*, 5117–5125. [CrossRef]
75. Aguilà, D.; Barrios, L.A.; Velasco, V.; Arnedo, L.; Aliaga-Alcalde, N.; Menelaou, M.; Teat, S.J.; Roubeau, O.; Luis, F.; Aromí, G. Lanthanide contraction within a series of asymmetric dinuclear [$Ln_2$] complexes. *Chem. A Eur. J.* **2013**, *19*, 5881–5891. [CrossRef]